An End-to-End Signal Strength Model for Underwater Optical Communications

Marek Doniec, Michael Angermann, *Member, IEEE*, and Daniela Rus, *Fellow, IEEE*

***Abstract*—In this paper, we present a generic model of signal strength in underwater optical communications. The model includes light sources, detectors, amplifier and detector circuitry, optics, as well as a simple extinction model of the water channel. The end-to-end model provides insights into optimization approaches for underwater optical modems and enables relative pose estimation between underwater optical transmitters and receivers. We instantiate our model to the AquaOptical model by determining its parameters and verifying the model prediction in a suite of pool experiments.**

***Index Terms*—Channel models, modeling, modem architecture, simulation and validation of point-to-point communications, software-defined modems, underwater optical communications.**

I. Introduction and Related Work

In this work, we develop an end-to-end model that helps to estimate the signal strength and resulting communication range in all directions. The model incorporates all components of the modem, including light sources, optics, detectors, amplifiers, and finally analog-to-digital converters. Our focus is to model the signal strength at any relative pose between the transmitter and the receiver. This includes the distances between the two and their individual poses.

The model supports underwater robotics in two ways. First, it enables estimation of the effects of the optical modem's components, providing a tool for examining how changes to individual components will affect range and coverage across larger angles with the goal of increasing robustness to pointing. Second, the information provided by the model can be used for location estimation. We showed previously that an AUV can use the optical signal strength to maintain position within communication range without external localization [1]. We believe that an optical signal strength model together with a Bayesian filter will enable enhanced localization.

Manuscript received November 22, 2012; revised June 21, 2013; accepted August 12, 2013. Date of publication September 18, 2013; date of current version October 09, 2013. This work was supported in part by the Multidisciplinary University Initiative (MURI) under Antidote Grant N00014-09-1-1031 and by the National Science Foundation (NSF) under Grants IIS-1133224 and IIS-1117178.

Associate Editor: J. Potter.

M. Doniec and D. Rus are with the Computer Science and Artificial Intelligence Laboratory (CSAIL), Massachusetts Institute of Technology (MIT), Cambridge, MA 02139 USA (e-mail: doniec@mit.edu; rus@csail.mit.edu).

M. Angermann is with the Institute of Communications and Navigation, DLR Oberpfaffenhofen, Wessling 82234, Germany (e-mail: michael.angermann@dlr.de).

Color versions of one or more of the figures in this paper are available online at http://ieeexplore.ieee.org.

Digital Object Identifier 10.1109/JOE.2013.2278932

This work builds on a wide body of research on underwater optical communications. Tsuchida *et al.* use optical communications to transmit measurement data from nontethered crayfish in a laboratory tank [2]. Schill *et al.* [3] and Vasilescu *et al.* [4] proposed optical communications for swarms of underwater vehicles. Dunbabin *et al.* proposed the use of optical communications for data muling where an underwater vehicle approaches a sensor and downloads data using a short-range but high-speed optical link [5]. Optical remote control of underwater vehicles was demonstrated by Farr *et al.* [6] and Doniec *et al.* [7].

Many of the systems implemented today have not been analyzed methodically to determine factors that influence their transmission ranges. Often, ranges were measured during field experiments, and the best range was reported. Some in-depth characterizations of transmission ranges have been performed in laboratories with large modem setups, but they are not field ready. Chancey measured the performance of the 10-Mb/s system with the transmitter and the receiver aimed at each other in a water tank at a distance of 4.6 m [8]. Hanson and Radic demonstrated a laser-based system capable of data rates of 1 Gb/s over a 2-m path in a tank with 36-dB extinction (absorbents were added to the water) [9].

Jaruwatanadilok proposed a channel model for optical underwater communications that uses the vector radiative transfer theory [10]. Giles and Bankman gave a model for computing achievable transmission range for a given setup when pointing both devices at each other. They considered both light source power and detector sensitivity, as well as extinction through the water [11]. Gabriel *et al.* proposed a model for simulating channel impulse response [12]. They used Monte Carlo simulations of their model to show that channel time dispersion is negligible in most practical cases, even for data rates of 1 Gb/s over a distance of 50 m with water turbidity equivalent to 7.5 e-folding lengths over 50 m. To our knowledge, no experimental validation of these results has been attempted, so far. Kedar and Arnon proposed a model for non-line-of-sight (NLOS) underwater optical communications [13].

This paper contributes the following:

- an end-to-end model of signal strength in underwater optical communications;
- an experimental evaluation of the model using the AquaOptical II modems, shown in Fig. 1 and previously published in [14];
- a discussion of the model in the context of the current state of the art in underwater optical communications.

The remainder of the paper is organized as follows. Section II presents the signal strength model. Section III gives an overview of AquaOptical II, the hardware used for experimental valida-

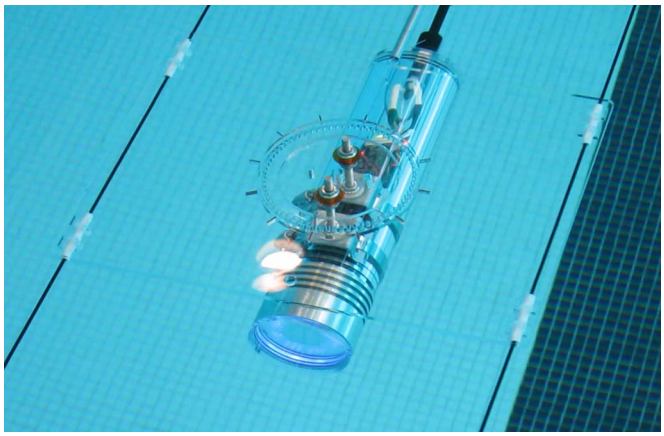

Fig. 1. The receiver is mounted to one end of the test setup. The receiver can be rotated in steps of 1° relative to the direct line of sight.

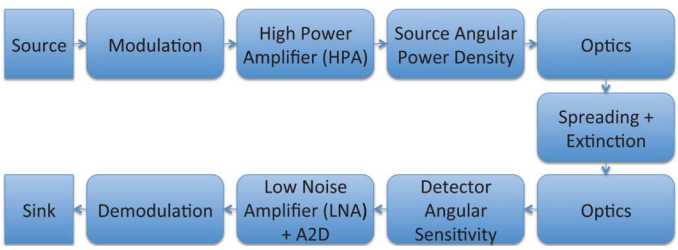

Fig. 2. Block diagram of the end-to-end signal strength model.

tion. We instantiate the model for AquaOptical II in Section IV by learning the relevant parameters. In Section V, we evaluate the predictions made by the model using AquaOptical II in the pool. We provide further discussions in the context of existing work in Section VI and conclude in Section VII.

II. Signal Strength Model

Fig. 2 shows the general layout of our model from the digital signal to be sent to the digital signal to be received. We will focus on the blocks starting from the high power amplifier to the low noise amplifier (LNA) because they have the most significant effect on optical signal transmission through water. The following model blocks will be treated in individual sections.

- The high power amplifier drives the optical source from logic level signals. We model it in Section II-A.
- We model how the signal is radiated in different directions, the source angular power density, in Section II-B.
- In Section II-C, we model the effect of source optics on the signal direction and intensity.
- The optical channel is modeled in Section II-D.
- Detector optics are modeled in Section II-E.
- Detector angular sensitivity is modeled in Section II-F.
- The LNA converts the sensed signal to detectable levels before it is digitized by the analog-to-digital converter. We model them in Section II-G.

A. High Power Amplifier

The high power amplifier (HPA) converts the modulated signal into a drive current for the transmit element, which is a light source. Currently, all optical modems deployed in water operate at bandwidths below 100 MHz, and most use amplitude modulation. The amplifiers used for this purpose are simple, and we approximate them as an identity function.

B. Source Angular Power Density

First, we look at the energy radiated from the light source and at how this energy is spread spatially. We consider point light sources. Let P_{total} be the total radiant power of the light source, let $\theta \in [0, \pi/2]$ be the angular displacement relative to the optical axis of the light source, and let I_{peak} be the peak radiant intensity of the light source (usually at $\theta = 0$). Let $f(\theta) \in [0, 1]$ be the relative intensity function. We make the assumption that $f(\theta)$ is rotationally symmetrical around the optical axis, but if necessary this constraint can be relaxed. The units are [W] for P_{total}, [W/sr] for I_{peak}, [rad] for θ, and [1] for $f(\theta)$. The relationship between these values is defined as

$$P_{\text{total}} = \int I_{\text{peak}} f(\theta_\Omega) \mathrm{d}\Omega \tag{1}$$

and by substituting $\mathrm{d}\Omega = \sin(\theta)\mathrm{d}\theta\mathrm{d}\varphi$, we get

$$\begin{aligned} P_{\text{total}} &= \int_{-\pi}^{\pi} \int_{0}^{\pi/2} I_{\text{peak}} f(\theta) \sin(\theta) \mathrm{d}\theta\mathrm{d}\varphi \\ &= 2\pi \int_{0}^{\pi/2} I_{\text{peak}} f(\theta) \sin(\theta) \mathrm{d}\theta. \end{aligned} \tag{2}$$

Solving for I_{peak} allows us to express the optical signal radiant intensity I_θ for a given angular displacement θ as

$$I_\theta = I_{\text{peak}} f(\theta). \tag{3}$$

C. Source Optics

1) Refraction: Before the optical signal reaches the water, it travels through multiple materials with different refractive indices. For example, in AquaOptical II, the optical signal first travels through air inside the modem. The signal then transitions from air to acrylic, the material from which the viewport is made. Finally, the signal transitions from the acrylic viewport into the water. Each transition can result in refraction, reflection, and transmittance. Refraction can have a focusing effect on the beam and may be desirable. Reflection is usually undesirable at these interfaces, as it prevents the signal from exiting the modem. Transmittance defines the amount of power that will pass through the material; the remainder is absorbed. All of these properties depend on the incident angle of the optical signal and on the refractive indices of the materials. Table I shows the refractive indices for the materials used in AquaOptical.

Snell's law defines the relationship between the incident angle θ_i, the transmitted angle θ_t, the refractive index of the medium that the signal is leaving n_1, and the refractive index of the medium that the signal is entering n_2, as

$$\frac{\sin\theta_i}{\sin\theta_t} = \frac{n_2}{n_1}. \tag{4}$$

Solving for the transmitted angle θ_t, we get

$$\theta_t = \sin^{-1}\left(\frac{n_1}{n_2}\sin\theta_i\right). \tag{5}$$

TABLE I
REFRACTIVE INDICES FOR SELECTED MATERIALS

Material	n at 470 nm
Air	1.00
Water	1.33
Acrylic	1.50
Quartz glass	1.46

2) Reflection: The reflected angle θ_r is equal to the incident angle θ_i. Using Fresnel's equations, we get the reflection coefficients (fraction of power reflected) for in-plane (R_s) and out-of-plane (R_p) polarizations

$$R_s = \left| \frac{n_1 \cos\theta_i - n_2 \cos\theta_t}{n_1 \cos\theta_i + n_2 \cos\theta_t} \right|^2 \tag{6a}$$

$$R_p = \left| \frac{n_1 \cos\theta_t - n_2 \cos\theta_i}{n_1 \cos\theta_t + n_2 \cos\theta_i} \right|^2 \tag{6b}$$

respectively. For unpolarized light, the reflection coefficient R is the average of these values, and, because of conservation of energy, the transmission coefficient T is one minus R

$$R = \frac{R_s + R_p}{2} \quad T = 1 - R. \tag{7}$$

3) Intensity Change: Refraction at a surface causes a beam to collimate when $n_1 < n_2$ or de-collimate when $n_1 > n_2$. This will increase or decrease the radiant intensity of the signal. This change in intensity can be computed by looking at the solid angle change at the boundary. In the case that the direction of light is oblique to the boundary between n_1 and n_2, the change of the solid angle Ω at the boundary is given in [15] as

$$d\Omega_1 = \frac{n_2^2 \cos\theta_t}{n_1^2 \cos\theta_i} d\Omega_2 \tag{8}$$

where Ω_1 is the incident solid angle and Ω_2 is the departing solid angle. This implies that the radiant intensity change across the boundary is

$$\frac{I_i}{n_1^2} = \frac{I_t}{n_2^2}. \tag{9}$$

D. Optical Channel

1) Spreading: In this paper, we consider a spherical spreading model with exponential decay. This model works well in clear waters, such as pool water, where scattering does not play a crucial role.

First, we consider power loss due to spherical spreading. Let r be the distance in [m] at which we measure the signal intensity. Using the radiant intensity I_θ from (3), we get irradiance $E_{\theta,\,\mathrm{spherical}}(r)$ at distance r, measured in [W/m^2]

$$E_{\theta,\,\mathrm{spherical}}(r) = I_\theta / r^2. \tag{10}$$

2) Extinction: Let c be the extinction coefficient for the water in which we are transmitting. In a general setting, this coefficient is the sum of the absorption coefficient a and the scattering coefficient b [12]. We consider waters in which scattering plays a negligible role and thus c tends toward a. This is true for clear waters but needs to be relaxed for waters with suspended particulate. Further, we assume that the coefficient is uniform across the entire length of transmission. This is a valid approximation for pool water but it can be imprecise for shallow ocean environments where currents cause inhomogeneity of the water quality. For extinction models that relax these assumptions, we refer the reader to the relevant literature [16]–[18].

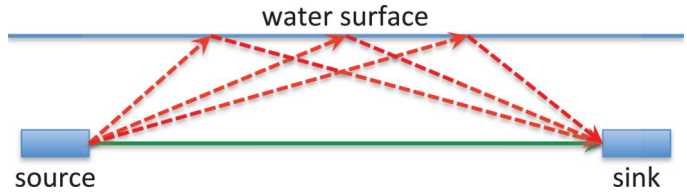

Fig. 3. Multipath: The optical signal travels from the source to the sink on the direct shortest distance route (solid green arrow) and via a multitude of reflections (dashed red arrows) from the water surface, seafloor, and other objects. The reflections travel a longer distance and thus arrive after the direct route signal, causing widening of transmitted optical pulses.

Beer's law gives the signal degradation at distance r caused by absorption as

$$S_r(r) = \exp(cr). \tag{11}$$

\

Combing spherical spreading with exponential decay we get a resulting irradiance of

$$E_\theta(r) = I_\theta \exp(cr)/r^2. \tag{12}$$

3) Temporal Signal Spreading Due to Multipath: In this section, we consider temporal spreading of pulses caused by multipath, as seen in Fig. 3. When light exits the transmitter (source) and travels toward the receiver (sink) a part will do so on the direction route (minimal distance path) but varying amounts of energy will reflect from objects such as the water surface, seafloor, and fish. These reflections travel a greater distance toward the receiver and arrive with a delay. This delay is detrimental to communication quality if it is on the order of magnitude of a symbol or longer. We now examine the magnitude of such delay that is caused by multipath. In particular, we examine the case of a single additional light path, computing what the worst case path can be for a given delay.

If c_{vacuum} is the speed of light in vacuum, then the speed of light in a solid with refractive index n_{material} is

$$c_{\mathrm{material}} = \frac{c_{\mathrm{vacuum}}}{n_{\mathrm{material}}}. \tag{13}$$

In the simplest case, this means that, if the signal has to travel an extra distance Δd, the exhibited temporal spreading is

$$\Delta t = \frac{\Delta d}{c_{\mathrm{material}}} = \frac{\Delta d n_{\mathrm{material}}}{c_{\mathrm{vacuum}}} \tag{14}$$

which in the case of water will amount to 100 ns for every 22.49 m. This means that even traveling a distance of 22.49 m only results in 100-ns temporal spreading. When considering a transmitted light pulse of duration t, this translates to a total received duration of the light pulse of up to $t+$ 100 ns when the maximal multipath is 22.49 m. Effectively, this means that if we

transmit symbols at 10 MHz (100 ns/symbol), then two neighboring pulses could fully overlap at the receiver side, given a reflected path that is 22.49 m longer than the direct light path. However, the signal will have been heavily attenuated by the additional 22.49 m it has to travel. Further, most underwater optical multipath is caused by reflection from tiny particles suspended in the water and is far smaller in magnitude, ranging from 1 to 10 ns for transmission ranges of up to 100 m [19], [20]. For these reasons, we choose to discard the effect of multipath for communication speeds below 10 Mb/s.

E. Detector Optics

The optics at the detector follow the same laws as the optics at the source. We need to again consider Snell's law [see (5)], Fresnel's equations [see (7)], and intensity change caused by refraction [see (9)].

F. Detector Angular Sensitivity

There are three commonly used optical detectors for sensing light intensity at low levels: 1) a conventional photodiode (PD); 2) an avalanche photodiode (APD); and 3) a photomultiplier tube (PMT). All three convert incident radiant power into current.[1] The output current I_{out} is linearly related to the incident power P_{in}. For a given sensor, this relationship, called responsivity, can be expressed as a constant

$$R_d = I_{\text{out}}/P_{\text{in}}. \tag{15}$$

The incident power can be computed from the signal irradiance arriving at the detector (10), the incident angle ϕ, and the area A_d (assumed flat) of the detector as

$$P_{\text{in}} = E_\theta(r) A_d \cos(\phi). \tag{16}$$

This yields a PD output current of

$$\begin{aligned} I_{\text{PD}} &= R_d P_{\text{in}} \\ &= R_d E_\theta(r) A_d \cos(\phi). \end{aligned} \tag{17}$$

Equations (16) and (17) hold for a cosine response system. Flat sensors with a fixed area, such as avalanche PDs and PDs without optics, exhibit cosine response. PMTs will exhibit a cosine response if they have a flat photocathode. However, even sensors with a flat active surface can have a different response function if optics are involved, such as with dome-shaped PDs, where a flat piece of silicon (active element) is embedded in a dome-shaped clear plastic housing that acts as a lens. For sensors with a different response, (16) and (17) need to be adjusted accordingly. In the most general case, the response function can be expressed using a general function f in a similar fashion to how we expressed source angular power density in Section II-B

$$P_{\text{in}} = E_\theta(r) f(\phi) \tag{18}$$

[1]This is true for all PDs, even when used in photovoltaic mode, where an additional resistor is used to generate and output voltage as opposed to output current.

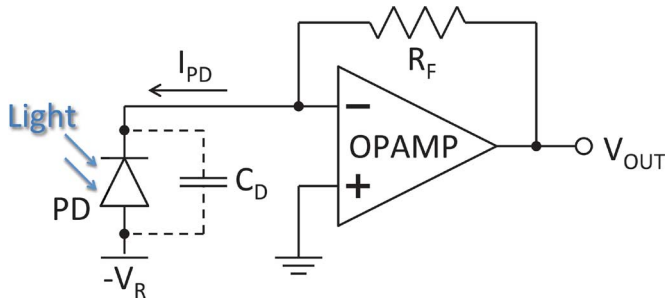

Fig. 4. TIA with PD. C_D is the parasitic PD capacitance, R_F is the feedback resistor to the operational amplifier (OPAMP), I_{PD} is the current through the PD (dark current and photon induce current), and V_{out} is the output voltage of the amplifier.

and

$$I_{\text{PD}} = R_d E_\theta(r) f(\phi). \tag{19}$$

In the case that the sensor exhibits a cosine response, we simply set

$$f(\phi) = A_d \cos(\phi). \tag{20}$$

G. Low Noise Amplifier

1) Amplification: The current produced by the PD generally needs to be amplified and converted into a voltage before it can be digitized by means of an analog-to-digital converter. This is typically done using a transimpedance amplifier (TIA). The schematic of a TIA is shown in Fig. 4. The TIA will convert the current from (17) into a voltage V_{out}, and this relation can be simplified as being proportional for frequencies below the bandwidth

$$V_{\text{out}} = R_{\text{TIA}} I_{\text{PD}}. \tag{21}$$

2) Bandwidth: Section II-F mentioned three different detectors (PDs, avalanche PDs, and PMTs). Two of the tradeoffs between these detectors are sensitivity and bandwidth. Detectors should be chosen such that they provide the bandwidth necessary and have the highest possible sensitivity, assuming constant noise.

Usually the more sensitive a device, the higher its intrinsic capacitance C_D, which results in higher bandwidth. However, lower intrinsic capacitance C_D results in higher diode impedance, which is computed as

$$X_c = \frac{1}{2\pi f C_D}. \tag{22}$$

The TIA uses an operational amplifier to amplify the incoming signal. The bandwidth f_{BW} of the TIA amplifier can be computed from the operational amplifier's gain-bandwidth (GBW) product and set gain $G = R_F/X_c$ as

$$f_{\text{BW}} = \frac{\text{GBW}}{G} = \frac{\text{GBW} X_c}{R_F} = \frac{\text{GBW}}{2\pi f C_D R_F}. \tag{23}$$

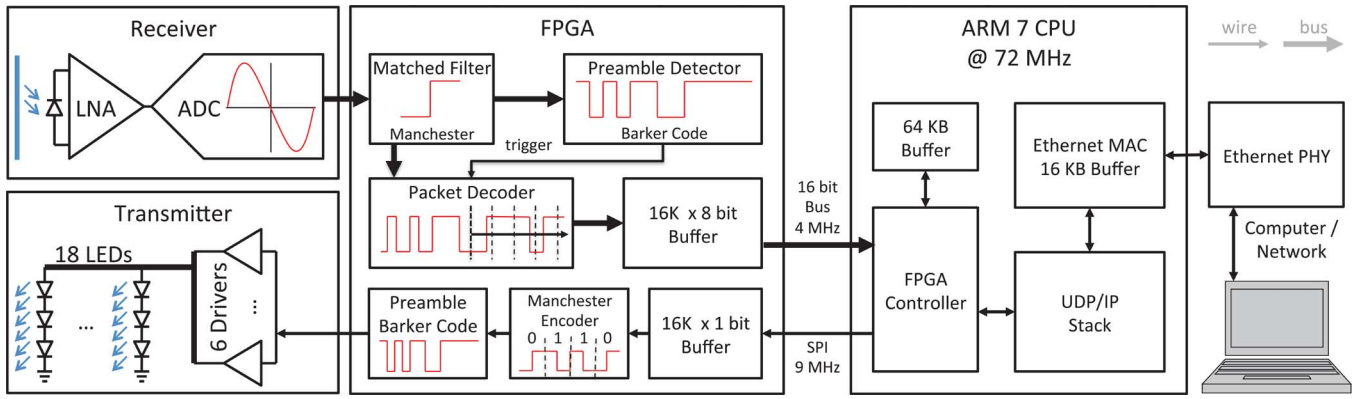

Fig. 5. System overview of AquaOptical II. The system consists of a transducer comprising the receiver and transmitter units, an FPGA that implements the physical and link layers, and an ARM 7 CPU that implements the MAC layer and Ethernet communications.

To get the bandwidth of the TIA for a PD with a given capacitance C_D and impedance X_c (22), we set $f_{\mathrm{BW}} = f$, which yields

$$f = \left(\frac{\mathrm{GBW}}{2\pi C_D R_F}\right)^{1/2}. \tag{24}$$

3) Noise: Photodetectors are subject to a range of noise types, including excess noise, Johnson–Nyquist ("thermal") noise, and shot noise, all of which play an important role in the design of photodetectors. For a practical application of these detectors, it is beneficial to subsume these noise types by one noise current spectral density figure at the chosen operating point. For most commercially available detectors, this is the figure provided in the devices datasheet.

Thus, the PD current noise is expressed as noise current spectral density $I_{N,\mathrm{PD}}$ in [A/$\sqrt{\mathrm{Hz}}$]. The current noise at a given frequency f is computed as

$$I_{N,\mathrm{PD}}(f) = I_{N,\mathrm{PD}} f^{1/2}. \tag{25}$$

An additional source of noise is Johnson–Nyquist noise originating from the feedback resistor R_F. At a frequency f and temperature T in Kelvin, this noise is equal to

$$I_{N,\mathrm{RF}}(f) = (4k_B T R_F f)^{1/2} \tag{26}$$

where $k_B = 1.38 \times 10^{-23}$ J/K is the Boltzmann constant. Both noise figures will be amplified by the TIA by the same factor as the signal, so they should be compared to the current signal exiting the PD.

III. AquaOptical II Hardware

We have instantiated the model described in Section II, using our underwater optical modem called AquaOptical II [14]. This section summarizes the AquaOptical II system.

A system overview of the AquaOptical II modem is shown in Fig. 5. It can be decomposed into three different parts: 1) a transducer comprising the physical receiver and transmitter units; 2) a field-programmable gate array (FPGA) that implements the physical and link layers; and 3) an ARM 7 central processing unit (CPU) that implements the medium access control (MAC) layer and Ethernet communications.

The ARM CPU forwards User Datagram Protocol (UDP) packets received through the Ethernet interface of AquaOptical II to the FPGA and triggers a packet transmit. The FPGA converts the raw bit stream into a transmit bit stream using Manchester coding where 0 b is encoded by a 01 sequence and 1 b is encoded by a 10 sequence. The FPGA then pre-appends a preamble that is used by the receiver for packet detection and clock synchronization. The preamble consists of a 13-b Barker code (111100110101 in binary). The resulting transmit bit stream is then forwarded to the transmitter hardware at 8 MHz. The transmitter uses drivers to convert the logic level signals into current pulses that drive the transmit light-emitting diodes (LEDs).

The receiver samples the medium for incoming packets. It contains an APD chosen for its high sensitivity and bandwidth. The output signal of the APD is amplified by an LNA and then digitized at a resolution of 12 b at a rate of 32 megasamples per second (MSPS). This stream is digitally convoluted with the expected shape by the FPGA on a per-sample basis to detect the packet preamble and to trigger a finite state machine called packet decoder. A matched filter in the shape of a step function (eight samples wide to match the data rate of 4 Mb) is used to decode the Manchester symbols. The packet decoder samples the sign of the matched step filter every eight samples once the preamble detector has triggered it. The first 16 b decoded this way are used to determine the length of the packet, and the remainder of the bits are stored in a buffer. This buffer is read by the ARM CPU and forwarded to the end user over UDP.

IV. Estimation of AquaOptical's Signal Strength

In this section, we instantiate the model described in Section II to the hardware described in Section III.

A. Source Angular Power Density and Source Optics

AquaOptical II uses Luxeon Rebel Blue LEDs (LXMLPB01-0023). The relative intensity graph of this LED is shown in Fig. 6. We used a polynomial fit of degree 6 (with R-squared $= 0.9999$) to facilitate further computation. The LED's typical luminous flux is reported as 70 lm at a drive current of 1 A. The relationship between luminous flux F and radiant power P for a fixed wavelength λ is defined as $F = 683$ lm/W $\bar{y}(\lambda)P$. The luminous efficiency $\bar{y}(\lambda)$ at 470 nm is specified as 9.1% [21]. This means that the LED's total radiant power is $P_{\mathrm{total}} = 1.126$ W. Solving (2) yields $I_{\mathrm{peak,\ LXMLPB01}} = 0.36$ W/sr in peak radiant intensity. AquaOptical II uses 18 Luxeon Rebel Blue LEDs to transmit. That means that AquaOptical's peak radiant

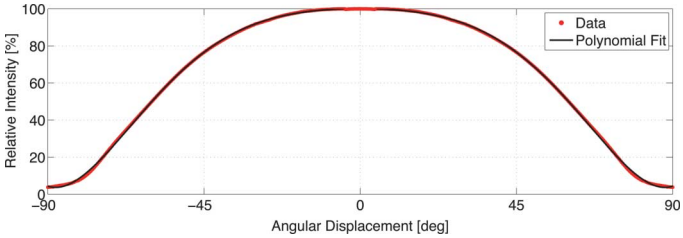

Fig. 6. Relative intensity of LED taken from data sheet (red) and polynomial fit (black). The x-axis shows the angular displacement in degrees; the y-axis shows the relative intensity in percent.

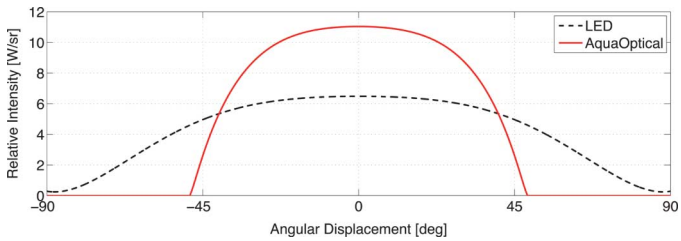

Fig. 7. Accumulated radiant intensity of the 18 LEDs inside the AquaOptical II modem (black dashed line) and the AquaOptical II modem itself (red line). The x-axis shows the angular displacement in degrees; the y-axis shows the radiant intensity in W/sr.

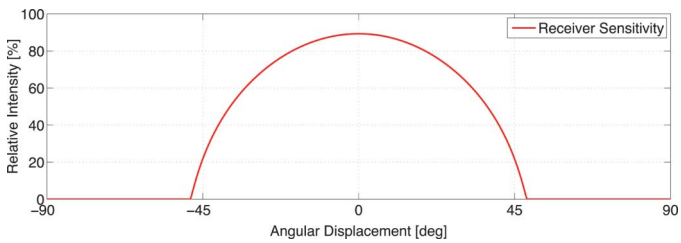

Fig. 8. Computed relative receiver sensitivity. The x-axis shows the angular displacement in degrees; the y-axis shows the relative intensity in percent.

power will be 18 × 0.36 W/sr. Further, our signal first transitions from air into acrylic, and then from acrylic into water, so we need to apply (5), (7), and (9). This yields the radiant intensity as shown in Fig. 7.

B. Receiver Sensitivity and Receiver Optics

AquaOptical II uses an APD that has a circular active area with a diameter of 5 mm. We are interested in the optical energy that arrives and is absorbed by the flat surface of the APD. The radiance arriving at the receiver is given in (12). The incoming signal needs to transition from water, through acrylic, air, an optical filter, and air again before it finally reaches the detector. It should be noted that we approximated the filter's refractive properties with those of glass, as no data for off-optical-axis performance is available. The computed relative angular sensitivity of the receiving modem is shown in Fig. 8.

The TIA used by AquaOptical is part of the APD module sold by Advanced Photonix (Ann Arbor, MI, USA) as part number SD197-70-74-661. The specifications of the module give a sensitivity $S = 9.5 \times 10^5$ V/W and a bandwidth of no less than 12 MHz. The noise current spectral density of the APD is $I_{N,\mathrm{APD}} = 0.8 \times 10^{-12}$ A/$\sqrt{\mathrm{Hz}}$, and the internal feedback resistor of the TIA is $R_F = 10$ kΩ. Our signal is sampled at $f = 32$ MHz. Using (25), we get the PD induced voltage output noise $U_{N,\mathrm{PD}} = 45$ μV. Using (26), we get the noise originating from the feedback resistor $U_{N,\mathrm{RF}} = 75$ μV (at 25 °C). Both of these values are well below the 1-mV quantization induced by the digital-to-analog converter.

C. Full AquaOptical II Signal Strength Model

Let d be the distance in meters between the two AquaOptical II modems, let θ be the transmission angle relative to the source's optical axis, and let ϕ be the incident signal angle relative to the detector's optical axis. We previously estimated the water in our pool to have an e-folding length of 36 m [22]. Let $c = 1/36$ m^{-1} be the absorption coefficient of pool water. Let $A_d = 19.64$ mm^2 be the detector area. We call $I(\theta)$ the source radiant intensity function of AquaOptical II, as depicted in Fig. 7, and $S(\phi)$ the detector relative angular sensitivity function, as depicted in Fig. 8. The power in [W] arriving at the detector is expressed as

$$P(\theta, \phi, d) = I(\theta)\frac{\exp(cr)}{r^2}S(\phi)A_d\cos(\phi). \tag{27}$$

Fig. 9(a) and (b) shows the received power for various spatial configurations of the transmitter and the receiver. In Fig. 9(a), the transmitter is fixed at the origin point right along the x-axis. The x- and y-axes denote the relative location of the receiver, which is always pointing straight at the transmitter ($\phi = 0$). Since the transmitter orientation is fixed, θ depends on the location of the receiver.

The opposite is true for Fig. 9(b). Here, the receiver is fixed at the origin point right along the x-axis. The x- and y-axes denote the relative location of the transmitter, which is always pointing straight at the receiver ($\theta = 0$). In this case, ϕ depends on the location of the transmitter.

V. Experimental Validation

We experimentally validate our model using the AquaOptical II modem [14]. We have designed a test fixture that allows us to arbitrarily position two modems relative to each other in the pool. The fixture is shown in Fig. 10. It allows us to translate the transmitter relative to the receiver to arbitrary distances (limited by the pool size, which is up to 50 m long) and to change both the receiver angle and the transmitter angle relative to the line of sight.

Our model is evaluated in clear pool water but can be extended to turbid waters such as the ocean environment by changing the water channel model. In the easiest case, this can be achieved by simply adjusting the extinction coefficient of the water.

A. Experimental Setup

Fig. 11 shows a schematic of the experimental setup. Two steel cables are tensioned between two opposing pool walls over a distance of 50 m. The cables are coated in black vinyl to reduce optical reflections and friction for the moving parts. The receiving modem is mounted to one of the pool walls using a specially designed rig. The mounting angle of the receiving modem is variable in the horizontal plane. This allows an arbitrary choice of the receiving angle. An acrylic plate is attached to the cables using two polytetrafluoroethylene (PTFE) bushings. Two bushings are used per cable to ensure stability. The transmitting optical modem is mounted to the bottom of the acrylic

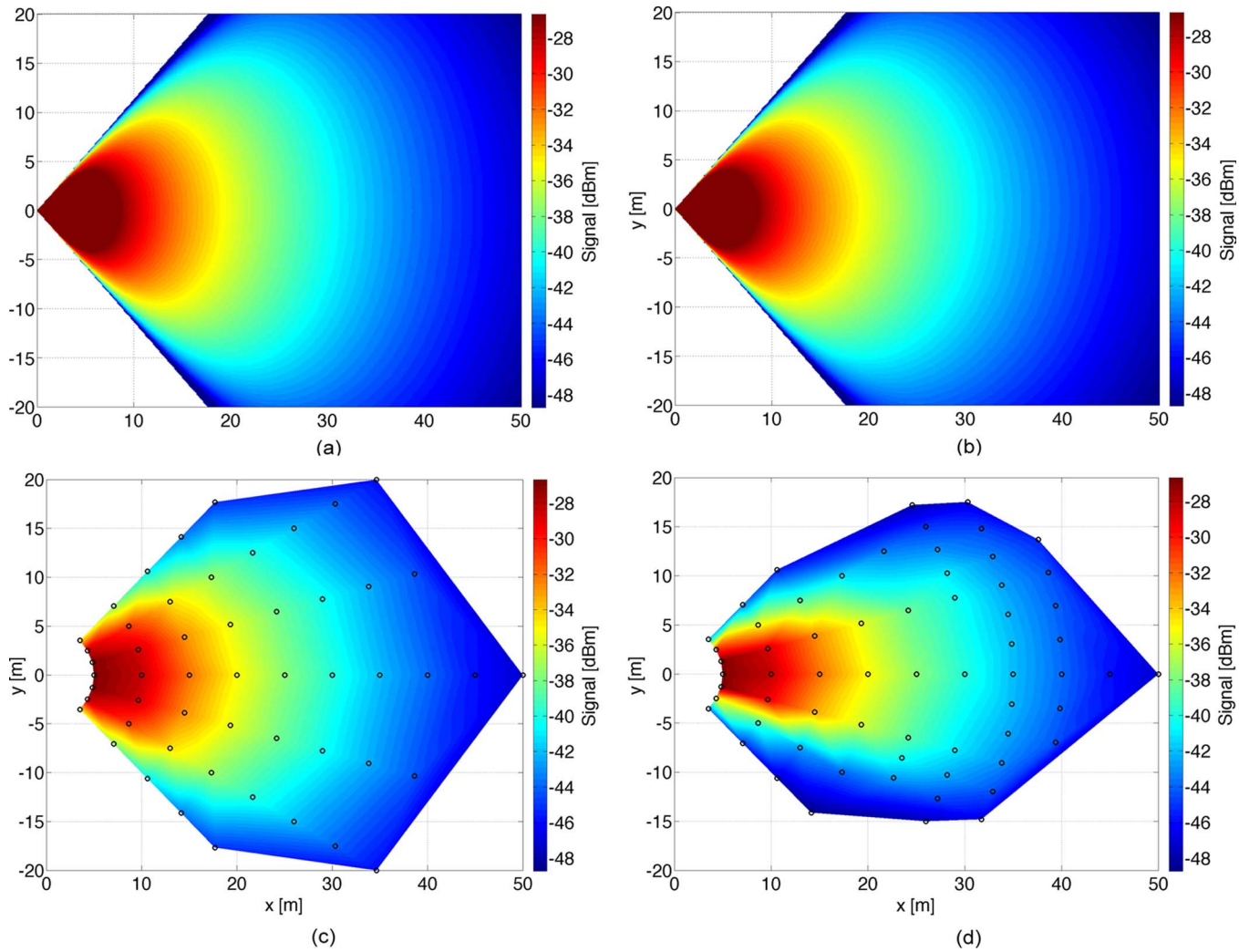

Fig. 9. Signal strength as measured at the detector: (a) and (b) simulation results and (c) and (d) experimental data. The signal strength is color coded from blue (-48.7 dBm, weak signal) to red (-26.7 dBm, strong signal). For each plot, the x- and y-axes show displacement of one of the modems relative to the other in meters. In the left plots (a) and (c), the transmitter is located at the origin and always points right (positive x-axis). The x- and y-axes show receiver displacement and the receiver is always pointing straight at the transmitter (θ varying, $\phi = 0$). In the right plots (b) and (d), the receiver is located at the origin and always points right (positive x-axis). The x- and y-axes show transmitter displacement, and the transmitter is always pointing straight at the receiver ($\theta = 0$, ϕ varying). The black circles show actual data points taken during the experiments; the data in between is interpolated. In (d), all measurement points are independent. In (c), data points were collected only for positive θ and the data were mirrored. (a) Model prediction: θ varying, $\phi = 0$. (b) Model prediction: $\theta = 0$, ϕ varying. (c) Experimental data: θ varying, $\phi = 0$. (d) Experimental data: $\theta = 0$, ϕ varying.

plate. The mounting angle of the transmitting modem is variable in the horizontal plane. This allows arbitrary choice of the transmitting angle. The acrylic plate together with the attached transmitting optical modem can glide along the cables, allowing the transmitter to be repositioned anywhere along the cables. This allows arbitrary choice of transmission distance between the receiver and the transmitter limited only by the pool size of 50 m.

B. Experimental Procedure

The transmitting modem is programmed to transmit symbols at a rate of 250 Hz. Each symbol consists of a 18-b code transmitted at a bitrate of 8 Mb/s. Thus, a single symbol is 4.5 μs long. The code is based on a 13-b Barker code and is displayed in Fig. 12. The receiver samples the incoming signal at 32 MSPS (four times oversampling) and applies a 72-sample wide matched filter to the incoming signal. The output of the matched filter is divided by the current signal power. When the resulting quotient exceeds a threshold of 0.8, a received symbol is registered and the peak power is recorded as a single signal strength measurement.

We call a specific set (α, β, d) of transmitter angle α, receiver angle β, and transmission distance d a data point. For each data point, the modems are moved to the correct configuration, and then all registered signal strength measurements are recorded for 30 s. Because of false negatives, when a sent symbol is not detected, it is possible that we record fewer than 30 s $\times$ 250 Hz $= 7500$ measurements for a specific data point. This is especially true for data points where the signal strength is weak, and, as a result, the symbols are harder to detect.

We collected two sets of data points. For the first set, we collected data points with the transmitting modem always aimed straight at the receiving modem $(\alpha = 0)$. For this set, we first move the transmitter to a fixed distance. The transmitter remains at this distance while we alter the receiver angle (β) and collect a 30-s-long data point each time. Then, we move the transmitter to the next distance. For the second set, we collected data points

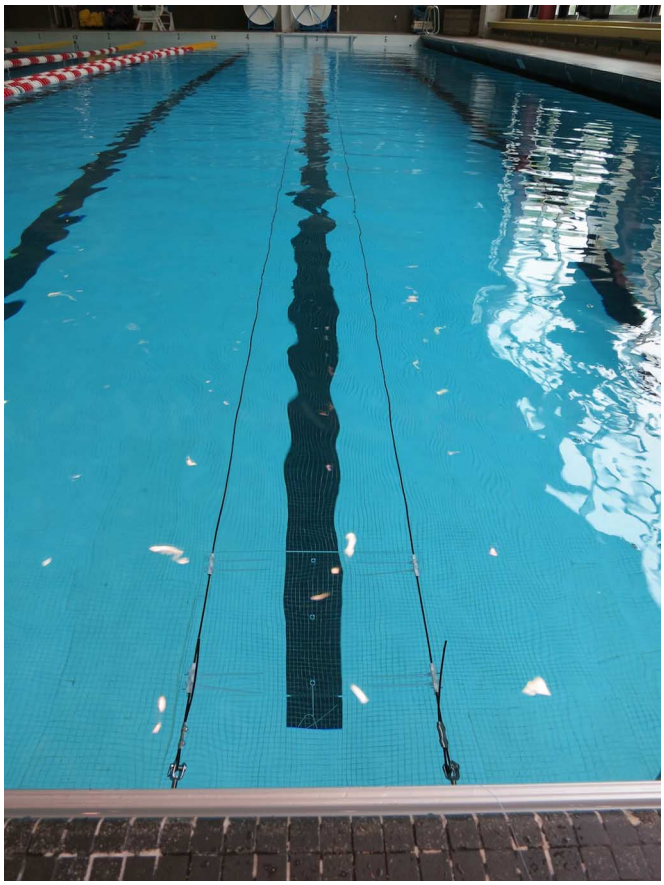

Fig. 10. Picture of the pool with the test setup. Two steel wires coated in black vinyl to minimize reflections are strained across the pool. A receiver is attached at one end, and a transmitter (Fig. 1) can travel on a cart attached to the wires. The cart is moved using a pulley system driven by a transparent fishing line. In the final setup, four additional wires form a 0.6 m by 0.6 m tunnel around the setup that is draped in black cloth to minimize reflections from pool walls and the water surface.

with the receiving modem always aimed straight at the transmitting modem ($\beta = 0$). For this set, we first set the transmitting angle (α) to a fixed value. We then move the transmitter to different distances and collect a 30-s-long data point each time. We repeat this for different values of α. The distances used for both sets range from 5 to 50 m in multiples of 5 m.

C. Experimental Results

First, let us consider the case in which both modems are aimed at each other ($\theta = \phi = 0$). Fig. 13(a) plots both the modeled signal strength and the experimental results for this case over transmission distances of 5–50 m. All measurements are reported in dBm.[2] Plotted in black is the model prediction. The blue dots correspond to the collected data. For distances between 10 and 50 m, the measurements agree with the model with a maximum error[3] of 0.35 dB. The only outlier is the measurement at 5 m, which is off from the modeled value by -5.24 dB. The reason for this is sensor saturation. Plotted as a horizontal dashed red line is the detector saturation, which is the equivalent of 3.3 V at the TIA output. Near this range, the amplifiers do not behave linearly and the signal becomes heavily distorted. The solid red horizontal line marks the detector threshold, which is set by the modem firmware to be 10 mV at the TIA output. The model predicts that this threshold is reached at 59.36 m.

Figs. 13(b) and (c) and 14(a) and (b) plot both the modeled signal strength and the experimental results for the cases with transmit and receive angles of $(\theta, \phi) \in \{(15, 0), (30, 0), (0, 15), (0, 30)\}$. The entire experimental data set is plotted as heat maps in Fig. 15(c) and (d). At a distance of 5 m, all data points are corrupted by detector saturation, which is why we do not include them in the following error analysis. Fig. 15 plots the maximum modeling errors for different values of θ and ϕ. For the cases where $\phi = 0$, the maximum errors over the distances of 10–50 m are 0.30 dB for $\theta = 15°$, 1.60 dB for $\theta = 30°$, and 2.92 dB for $\theta = 45°$. For the cases where $\theta = 0$, the maximum errors over the distances of 10–50 m are 0.89 dB for $\phi = -15°$, 0.35 dB for $\phi = 0°$, and 0.39 dB for $\theta = 15°$. For angles ϕ great than 30°, the maximum errors are between 6 and 10.47 dB.

D. Discussion

The experimental data are within 0.89 dB of the model prediction for values of $|\theta| \leq 15°$ and $|\phi| \leq 15°$. This means we are correctly predicting signal strength to within a factor of 23%. The transmitter model error grows to 2.9 dB at $\theta = 45°$. At this point, it is off by a factor of 2, but it still captures the right order of magnitude. The receiver model, on the other hand, is off by a factor of 10 at 45° and does not perform much better at 30°.

Potential sources of an error are the pool walls and water surface because they can reflect the signal and cause distortions to the measurements. However, such an error would cause an increase in measured signal strength. Since we observed mostly lower experimental measurements than what the model predicted, it is unlikely that the walls were a major source of errors.

We believe that more likely causes are yet unmodeled geometrical constraints in the modems. For the transmitter, the LEDs are close to the viewport, and there is sufficient space on the sides for the signal to spread, thus we observe a good fit. However, in the receiver, the stack of viewport, filter, and screens to mask ambient light creates shadows as the light enters the receiver at an angle. This is essentially equivalent to the sensor surface sitting at the end of a tube whose diameter is roughly the same as the length, preventing light that arrives at an angle to reach the sensor area directly. This effect is amplified by the refraction at the viewport, which increases the incident angle significantly. For example, a signal arriving at 30° is refracted by the viewport to travel at an angle of 41.8° inside the modem. This is likely to be at least partially occluded by the screens inside the detector. Additionally, we have not yet modeled the behaviors of the fluorescence bandpass filter used, which starts reflecting a large portion of the signal already at low angles.

VI. Discussion in the Context of Current Knowledge

Our approach to underwater communication modeling followed by instantiation to physical hardware is general and can

[2]Absolute power referenced to 1 mW:1 mW = 0 dBm, 1 μW = -30 dBm.

[3]The relative difference between two absolute power values is expressed in decibels.

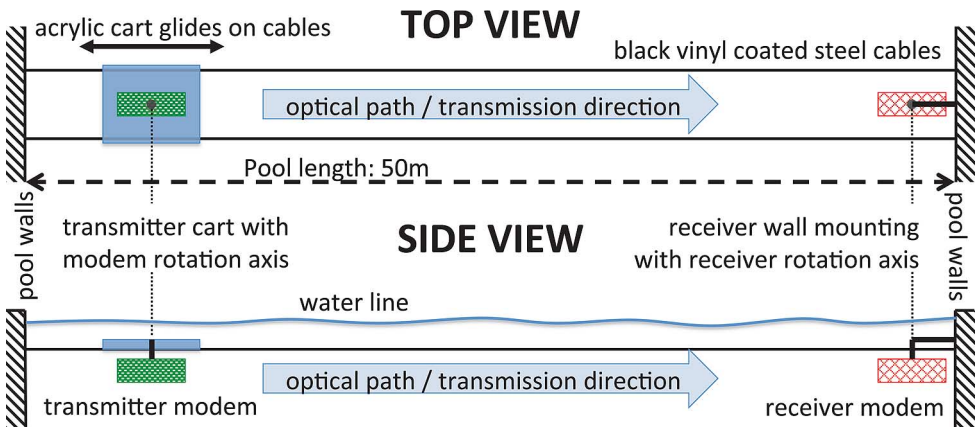

Fig. 11. Experimental setup. Two steel cables are tensioned between two opposing pool walls over a distance of 50 m. The cables are coated in black vinyl to reduce reflections and friction. The receiving modem is mounted to one of the pool walls. The mounting angle of the receiving modem is variable in the horizontal plane to allow arbitrary choice of receiver angle. An acrylic plate is attached to the cables using two PTFE bushings per cable to ensure stability. This plate can be repositioned to any distance from the receiver. The transmitting optical modem is mounted to the bottom of the acrylic plate. The angle of mounting of the transmitting modem is variable as well to allow arbitrary choice of the transmitter angle.

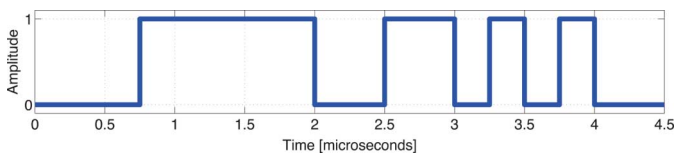

Fig. 12. Header code sent by the transmitter and used in the matched filter by the receiver.

be applied to many of the devices developed in the recent past by the underwater communication community. In this section, we provide a detailed review of the systems we believe are most relevant and amenable to this approach. We hope that the approach described in this paper can provide a unifying framework for characterizing the performance of the devices and establishing tradeoffs between them.

A. Woods Hole Oceanographic Institution (Woods Hole, MA, USA)

Farr *et al.* estimate the required transmit power required to maintain a bit error rate (BER) of 10^{-6} for various data rates and distances [23], [24]. Their model combines absorption and scattering losses in water into a single constant attenuation loss e^{-cR} for a distance R. This is Beer's law. They assume an e-folding length of 36 m. For a system using LEDs and a PMT, they compute a required transmit power of 300 mW for a data rate of 10 Mb/s at 100 m with a 13.4-cm large receiver aperture and 90° transmitter beam. If the receiver aperture is reduced to 5 cm and the transmitter beam to 10°, the required power for the same data rate and distance drops to 6.5 mW. They argue that multipath and signal spreading has no significant effect on data rates below 10 Mb/s. Further, they propose that background noise caused by bioluminescence and Cherenkov radiation is low enough that it does not interfere with the signal. They create a test setup with six potted LEDs transmitting in a 2π sr hemisphere and a bi-alkali PMT receiver with quantum efficiency of 20% and a gain of 10^7, driven at 400–500 V. They test their system at the Woods Hole Oceanographic Institution (WHOI, Woods Hole, MA, USA) docks over a distance of 10 m by sending 1-, 5-, and 10-MHz square pulse trains and record signal-to-noise ratio (SNR) values of 30–35 dB.

Pontbriand *et al.* use a 43.2-cm diameter glass sphere to improve the field of view [25]. The sphere houses a PMT, and they use an external power source and feed the output signal to an external digitizer. Their system communicates at rates up to 5 Mb/s and distances up to 200 m at an e-folding length of 40 m. In turbid water with an e-folding length of 0.8 m, they achieve 1 Mb/s. Their tests are performed in Bermuda and at the Woods Hole dock.

In [26] and [6], Farr *et al.* describe the optical telemetry system (OTS) with which they download 20 MB of data over a 5-Mb/s link at a range of 80 m. They report communication at a data rate of 10 Mp/s at a distance of 108 m, 5 Mb/s at distances of up to 128 m, and 1 Mb/s at distances of up to 138 m. Additionally, they provide optical signal power measurements at various distances. For a source power of 15–20 W, they report incident power of approximately 2×10^{-7} W at 50 m, 10^{-8} W at 100 m, and 2×10^{-9} W at 150 m.

Camilli *et al.* [27] discuss the application of optical communications to ocean observatories and claim that it allows for 10 Mb/s with ten or more e-folding scales resulting in communication distances of 100–200 m. They categorize optical communications as permitting data rates on the order of 1 Mb/s at distances close to 100 m at an energy expenditure of 40 000 b/Joule.

We can plug the values reported by Farr *et al.* into our signal strength model to compute the irradiance at the receiver. If we assume that their transmitter emits 15 W evenly over a hemisphere and the water's enfolding length to be 40 m, we can compute the irradiance according to (12) as 270 μW/m^2 at 50 m, 19.6 μW/m^2 at 100 m, and 2.5 μW/m^2 at 150 m. A least squares fit to the received power values reported by Farr *et al.* yields a receiver aperture area of 7.3×10^{-4} m^2 equivalent to a diameter of 3 mm. This value is within the bounds of commonly used PMT. In comparison, our AquaOptical II system utilizes an APD because of its increased quantum efficiency [28]. It has a diameter of 5 mm. AquaOptical II can decode signals of at least 10^{-8} W

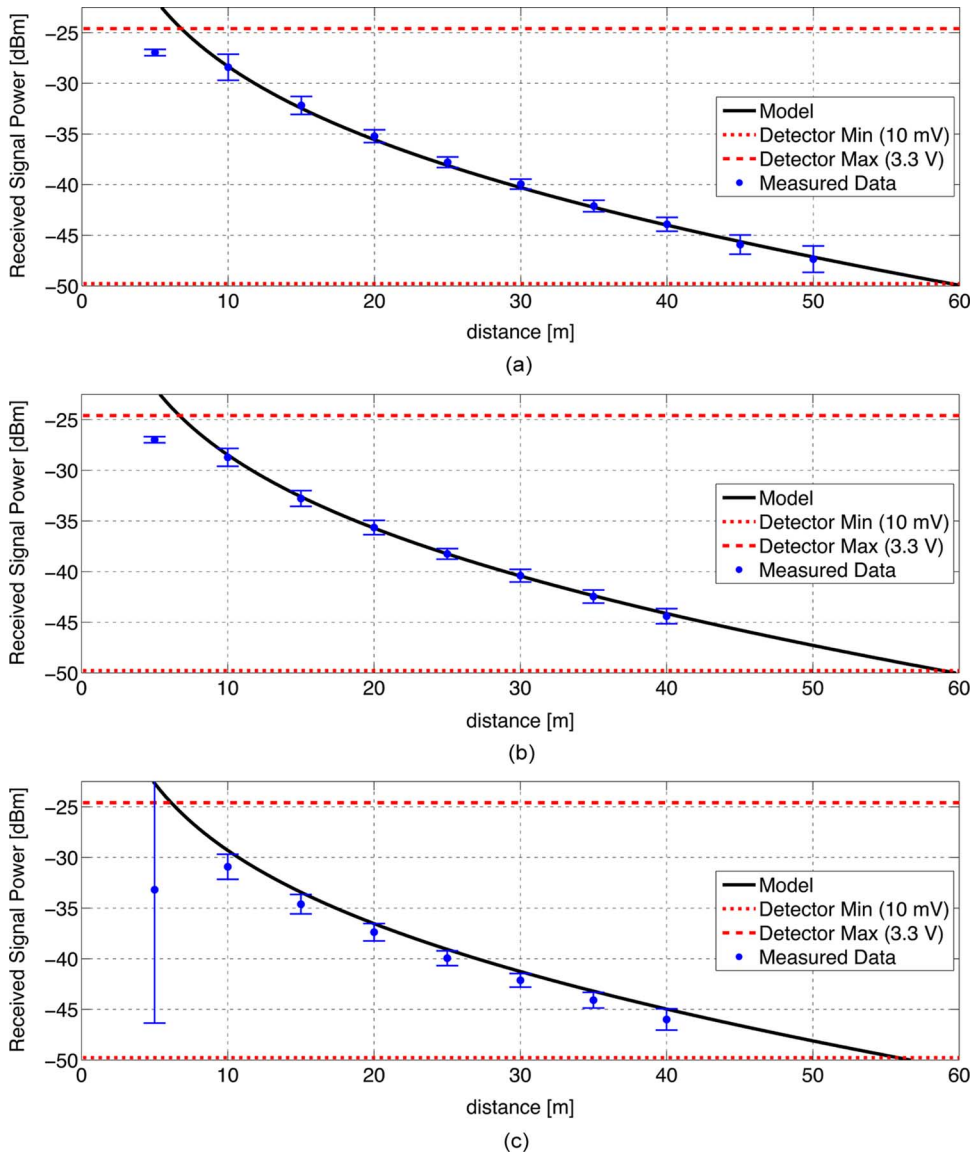

Fig. 13. Modeled signal strength and experimental data. The x-axis shows distance in meters. The y-axis shows received signal strength in decibels. The black line shows the output of the model from Section IV-C. The red lines mark the detection threshold (solid) and saturation (dashed). Experimental data are plotted blue with 3σ error bars. (a) Both modems are aimed straight at each other ($\theta = \phi = 0°$). (b) Transmission angle $\theta = 15°$, reception angle $\phi = 0°$. (c) Transmission angle $\theta = 30°$, reception angle $\phi = 0°$.

[10 mV at the digital-to-analog converter (DAC)]. The reduced sensing area thus results in an operating distance of 50 m at a data rate of 4 Mb/s. However, our device has a lower energy expenditure of 400 000-b/Joule radiant power. This results in 120 000 b/Joule when including the total combined power consumption at the transmitter and the receiver. Further, the system can cope with ambient light allowing operation near the water surface.

B. North Carolina

In [8], Chancey uses an amplifier to drive a 1-W LED with a 10BaseT Ethernet signal and a PD on the receiving side that converts the incoming light pulses back to the 10BaseT range. His design is based on an existing free-space optical communication implementation called the reasonable optical near joint access (RONJA). He tests his system in a water tank over a distance of 4.6 m and extrapolates that the potential link distance is 16 m.

In [29], Cox uses a 405-nm laser for transmission and the miniature Hamamatsu R7400U PMT in conjunction with an AD8015 variable gain amplifier (VGA) on the receiving side. His system is tested using a water tank with reliable communication at 500 kb/s.

Using the same laser diode and a PNZ334 PD and a personal computer (PC) for postprocessing, Cox *et al.* show that the use of forward error correcting (FEC) codes achieves a BER of 10^{-4} at SNR levels 8 dB lower than without FEC [30]. They use ON–OFF keying (OOK) in a return-to-zero (RZ) coding to transmit data at a rate of 500 kb/s through water in a 3.66-m-long tank. They vary the SNR by changing the attenuation coefficient of the water through the addition of Maalox. Their uncoded stream achieves approximately a BER of 0.5 at 6.5-dB

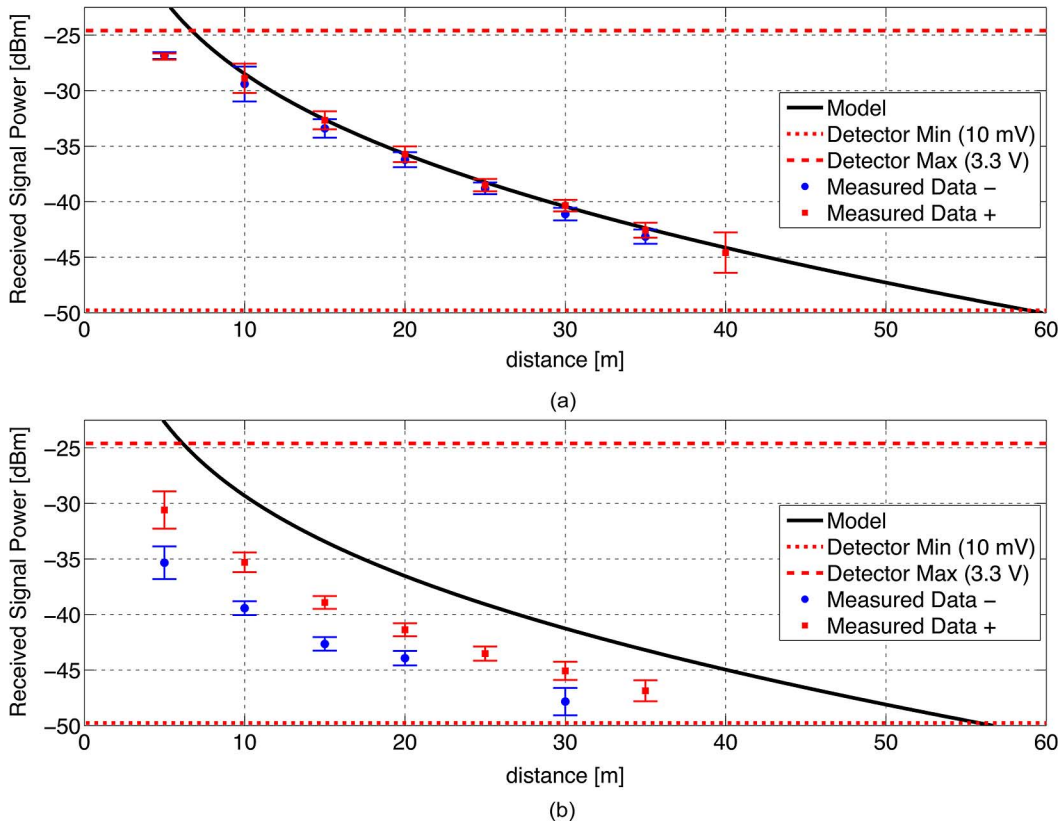

Fig. 14. Modeled signal strength and experimental data. The x-axis shows distance in meters. The y-axis shows received signal strength in decibels. The black line shows the output of the model from Section IV-C. The red lines mark the detection threshold (solid) and saturation (dashed). Experimental data are plotted blue (negative reception angle) and red (positive reception angle), each with 3σ error bars. (a) Transmission angle $\theta = 0°$, reception angle $\phi = 15°$. (b) Transmission angle $\theta = 0°$, reception angle $\phi = 30°$.

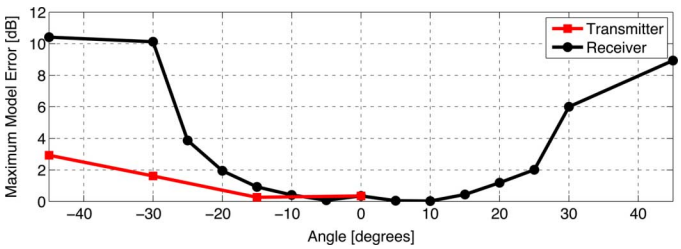

Fig. 15. Maximum model errors when compared to experimental data for distances between 10 and 50 m. The x-axis shows the angle (θ for the red and ϕ for the black line). The y-axis shows the error in decibels. The red line plots the errors when the transmitter angle was changing. The black line plots the errors when the receiver angle was changing.

SNR, 10^{-1} at 8.5 dB, 10^{-2} at 12 dB, 10^{-3} at 16 dB, and 10^{-4} at 19 dB. When using a (255, 129) Reed–Solomon (RS) code, they achieve a BER of 10^{-4} at 11-dB SNR.

Simpson *et al.* show through simulation that, for a BER of 10^{-6}, the (255, 223) RS code provides an SNR improvement of 4 dB and the (255, 129) RS code provides an SNR improvement of 6 dB [31]. They transmit data through a water tank using a 3-W LED (CREE XR7090) at 470 and 525 nm. They use two setups: in one, they transmit over a length of 3 m through turbid water (4+ e-folding lengths), and in the other, they transmit over a length of 7.7 m through less turbid water (one to two attenuation lengths). A PMT is used to receive the first (weak) signal and a PD to receive the second (stronger) signal. Their equipment is battery powered, but the signal is digitized at 100 MSPS (20 times oversampled) using external equipment. They use a matched filter to maximize SNR and early/late gate symbol synchronization. Their system achieves 5-Mb/s throughput.

In [32], Simpson *et al.* propose a two-transmitter two-receiver spatial diversity system. They use a 200-mW, 405-nm laser together with a beam splitter to generate two parallel optical beams separated by 10.2 cm. Two 25.4-mm lenses focus the light onto two Thorlabs PDA36A amplified photo detectors. They investigate the use of equal gain recombination and maximum recombination for the two received signals. They transmit through a water tank into which they inject bubbles to generate interruptions of the optical beam. They show that their setup, using a data rate of 500 kb/s, reduces fading-induced errors by a factor of 10, when compared to a single 200-mW transmitter, single-detector system.

Another novel approach is proposed by Cox *et al.* in [33]. They designed a microelectromechanical system (MEMS) Fabry–Pérot-modulated reflector that is used to modulate an existing optical beam. The reflector can be attached to a node or a vehicle, and a querying node or a vehicle shines an optical beam on it and receives the reflected and modulated signal. They use a 20-mW, 532-nm laser and a Thorlabs PDA36A amplified photodetector at the querying node. They demonstrate data rates of 500 kb/s to 1 Mb/s using quadrature phase-shift keying (QPSK) through a 7.7-m-long tank corresponding to 2.5 e-folding lengths. Their system uses little power for the reflector but requires the beam to travel twice the transmission distance.

In [34], Cox *et al.* implement a complete duplex communication system based on 410-nm, 30-mW laser diodes and a Thorlabs PDA36A amplified PD receiver with a 51-mm collection lens. They use two Ettus Research Universal Software Radio Peripheral (USRP) signal acquisition boards together with GNU radio[4] software to generate the transmitted signal and to decode the incoming signal. Tests are conducted in a 3.66-m-long tank, and different attenuation coefficients are achieved with the addition of Maalox to the water. When using 1-Mb/s binary phase-shift keying (BPSK), they measure the BER to be 0.2 at a SNR of 4 dB, 10^{-2} at 7 dB, 10^{-3} at 9 dB, and 10^{-4} at 10.5 dB. A duplex networking test is performed using 1-Mb/s Gaussian minimum-shift keying (GMSK) modulation. They achieve round trip latencies of below 10 ms at up to 5.3 e-folding lengths.

With AquaOptical II, we implemented a two-layered coding scheme that can be made invisible to the user. We use a reconfigurable RS inner code with a system Luby Transform (LT-code) outer coder. AquaOptical II exhibits a BER of 10^{-6} at a receiver power level of -41 dBm and a BER of 10^{-4} at -46 dBm. By default, we use a (256, 223) RS code capable of correcting 16-B errors. We chose to utilize LED light sources instead of lasers to maintain eye safety for human operators and to reduce pointing requirements. Because of its large aperture of 7 cm and nonfocused beam, AquaOptical II implicitly implements a spatial diversity system that achieves low bit errors due to air bubbles and other scattering agents in the water.

C. Naval Air Warfare Center (NAVAIR), Patuxent River, MD, USA

Cochenour *et al.* use laser modulation with a 70-MHz radio-frequency (RF) carrier and BPSK to achieve error-free communication at a data rate of 1 Mb/s through highly turbid water [35]. They use a frequency-doubled diode-pumped solid-state laser with a wavelength of 532 nm and an output power of 3 W. This continuous-wave (CW) optical signal is modulated using an electro-optic modulator. The optical power transmitted into the water is approximately 500 mW after losses through the optical modular and other optical elements. The detector is a PMT with a 51-mm aperture, corresponding to 18° field of view. The received RF signal is bandpass filtered at 70 MHz and amplified by a 30-dB LNA and a 50-dB VGA. An IQ demodulator extracts the I and Q channels, which are lowpass filtered and digitized using a National Instruments data acquisition (DAQ) card. The system is tested in a 3.6-m water tank with the turbidity of the water controlled through the addition of Maalox. A pseudorandom 1024-b sequence is used to measure bit errors. The transmitted signal is recovered error free even at a turbidity that is equivalent to 90 e-folding lengths at 3.6 m. The phase error for the BPSK never exceeds 3°. However, the authors point out that this surprisingly good result might be due to the small geometry of the tank.

In [36], this work is extended to quadrature phase-shift keying (QPSK), 8 phase-shift keying (8-PSK), 16 quadrature amplitude modulation (16-QAM), and 32-QAM. Tests are conducted again in a 3.6-m water tank with water turbidity adjusted to 8.4 e-folding lengths for the length of the tank. Data are sent at 10^6 symbols per second, resulting in data rates from 1 Mb/s for BPSK to 5 Mb/s for 32-QAM. Two transmission powers are used in the tests. With a signal power of 750 mW entering the water, all modulation schemes yield BER of 10^{-5} or better. When a signal power of 75 mW is used, BPSK yields BER 0, QPSK yields BER 10^{-3}, 8-PSK yields BER greater than 0.1, and 16-QAM and 32-QAM fail to establish a link.

In [37], Cochenour and Mullen investigate the use of a diffuser to de-collimate the laser beam. The goal is to allow communication with less pointing accuracy or even NLOS links. Measurements are taken by sending 10-ns laser pulses at 100 MHz and using a PMT with 1-GHz bandwidth. The pulse shapes are examined for a collimated laser beam and for a laser beam that has passed a diffuser creating a beam with a 20° field of view. The authors conclude that the NLOS link requires at least 30 dB more transmission power to achieve a similar signal level at the receiver.

Through the use of LEDs, the light emitted from AquaOptical II is inherently de-collimated. In comparison to the above work, the LEDs have a lower bandwidth which prohibits RF modulation. However, we utilize Barker codes for packet detection which separates the signal from the background noise and Manchester coding for bits which is related to BPSK. The use of LEDs allows for smaller and cheaper devices, increased eye safety, and reduced aiming requirements.

D. University of Genoa, Genova, Spain

Anguita *et al.* implement a transmitter that uses 12 LEDs arranged on a circle to transmit omnidirectionally in the plane [38]–[40], [41]. In two different implementations, they use two different LEDs. The first is a Ledman LL1503PLBL1-301 with optical power 15 mW and a 30° field of view (50% power angle). The second is an Everlight Electronics (Carroliton, TX, USA) DLE-038-045 with optical power 20 mW and a 30° field of view. They propose an 18-LED omnidirectional transmitter design in the shape of an octahedron. Their receiver consists of a Hamamatsu Corporation (Middlesex, NJ, USA) S5971 APD with an area of 1 mm^2 and a sensitivity of 0.2 A/W at 470 nm. The output signal is fed through a 10 kHz to 20 MHz bandpass filter, an amplifier with automatic gain control (AGC) based on LT1006, and a comparator to digitize the incoming signal using thresholding. The optical physical (PHY) layer is implemented inside an FPGA on a Digilent Spartan 3 development board. They test their system with a square wave at distances of up to 2 m and report the voltage swing after the AGC. They show that their AGC allows for pulse detection from distances of a few centimeters to 10 m in air. Using 4- and 16-pulse position modulation (PPM), they report a data rate of 100 kb/s over a distance of 1.8 m in a clean water tank.

The analog front end of AquaOptical II digitizes the received signal at a resolution of 12 b at 32 MSPS as opposed to the threshold filter described above. This allows us to implement a wide variety of available coding schemes for the PHY layer, which is also housed inside an FPGA. An additional ARM processor is used by AquaOptical II to implement the MAC layer.

[4]http://gnuradio.org

E. Commercial

Ambalux Corporation (Tucson, AZ, USA) manufactures a commercial optical modem with a data rate of 10 Mb/s [42]. They claim transmission distances of up to 40 m. Their modem interfaces over 10BaseT Ethernet and allows TCP/IP and UDP communications. Power is provided externally, with the transmitter consuming 36 W and the receiver consuming 7.2 W. The units are rated to a depth of 60 m. Abalux Corporation claims that higher bandwidths up to 1 Gb/s and larger operating depths up to 6000 m can be achieved. However, no such device is currently available to the public.

Baiden *et al.* used an Abalux Corporation modem in [43] and [44]. Their tests were performed at Long Lake in Sudbury, ON, Canada, and in the pool. They achieved 9.69 Mb/s over a distance of 11 m. In the pool, they establish an 8.2-Mb/s link at distances up to 21 m. Further, they present a novel spherical transmitter and a receiver capable of transmitting at data rates of 20 Mb/s over a distance of 10–11 m. The same spherical transmitter/receiver pair achieves a data rate of 115 kb/s at distances of 15 m in the field.

The devices developed by Baiden *et al.* are being commercialized by Penguin Automated Systems, Inc. (Naughton, ON, Canada) [45].

In comparison, AquaOptical II consumes 24 W at the transmitter and 10 W at the receiver when operating at full throughput over distances of 50 m. We currently allow for UDP connections over a 10BaseT Ethernet connection. Because of its reconfigurable nature, AquaOptical II can be easily adapted to use TCP/IP or other protocols.

F. Other

Hanson and Radic demonstrated a laser-based system capable of error-free data rates of 1 Gb/s over a 2-m path in a water-filled 2-m-long pipe with 36-dB extinction [9]. The pipe had an inside diameter of 10.16 cm, and a layer of black mash filter cloth was cemented to the inside wall of the pipe to reduce parasitic light scattering. Maalox absorbents were added to the water. This corresponds to 8.3 e-folding lengths. Their system uses a 7-mW, 532-nm laser generated from a 1064-nm source that is optically pumped using a ytterbium-doped fiber amplifier and frequency doubled with a periodically poled lithium niobate (PPLN) crystal. They use an avalanche PD as a receiver.

Chen *et al.* use a 532-nm yttrium aluminium garnet (YAG) laser to generate 10-ns-wide, 200-mJ pulses [46]. This corresponds to a 2-MW laser and, as a result, they can only generate pulses at 50 Hz. They use 256 PPM with a bin size of 10 ns. They successfully transmit data through a 50-m-long water tank.

Hagem *et al.* implement a low-cost and short-range unidirectional optical modem [47]. They use frequency-shift keying (FSK) at a data rate of 2.4 kb/s with modulation frequencies of 10 and 12 kHz. Their implementation consists of a 520-nm, 1.5-mW PD with a 70° field of view and an optical detector with a sensitivity of 0.3 A/W. They achieve error-free communication at distances up to 1.1-m underwater without bubbles and up to 0.7 m with bubbles.

Lu *et al.* use a RL5-G13008 super-green LED, with a wavelength of 520 nm and a maximum power of 120 mW, and a Silonex SLD-BG2A PD together with a bandgap filter to reject infrared wavelengths [48]. The transmitter had a field of view of 90°, and the receiver had a field of view of 120°. They use a 32-b gold sequence as a packet preamble for clock synchronization. They tested their system in a pool at night to avoid ambient light. The system detected 80% of the transmitted packets at a communication distance of 10 m. Over 95% of the packets were detected at 6 m and below. The BER was approximately 1.8×10^{-3} at 2 m, 3.5×10^{-2} at 6 m, and 0.5 at 10 m.

Brundage implements a unidirectional communication system using a 465-nm, 4.8-W titan blue lighting engine (NT-52B1-0469) and a PC10-6B PD manufactured by Pacific Silicon Sensor (Westlake Village, CA, USA) [49]. The light source has a 22° field of view, and the system needs to be aimed. The light source is driven by a computer using a metal–oxide–semiconductor field-effect transistor (MOSFET), and the detector uses a simple comparator setup to threshold the incoming signal. The author does not specify the protocol. The system achieves error-free communication at 1 Mb/s at distances up to 13 m. Up to 3 Mb/s were possible with unspecified amount of bit errors.

Schill *et al.* designed a small optical communication transceiver for a swarm of submersible robots [3]. They use an IrDA PHY layer based on the MCP2120 IrDA encoder/decoder chip. Their receiver uses a SLD-70 BG2A PD together with a MAX3120 for amplification and filtering. They examine three different Luxeon III LEDs for transmission: blue (460 nm, 733 mW), cyan (490 nm, 560 mW), and green (520 nm, 165 mW). They use a byte-oriented Universal Asynchronous Receiver/Transmitter (UART) serial interface at 57 600 b/s. They test their system in air and achieve reliable communication at 1.71 m for 460 nm, 2.02 m for 490 nm, and 1.49 m for 520 nm. All three wavelengths establish a link when tested in a pool at ranges up to 1.7 m.

G. MIT/AquaOptical

Vasilescu *et al.* design and implement an optical modem capable of optical data muling [50]. They use a Luxeon 5 LXHL-PM02 LED with 532-nm, 700-mW radiant power. The receiver consists of the PIN PD PDB-C156 with a surface area of 8 mm^2. They implement digital pulse interval modulation (DPIM) with 2 b per pulse at an average data rate of 320 kb/s. The communication range of their system is 2.2 m point to point with a cone of 30°. Using a collimating lens, they demonstrate error-free communication through clear water over a distance of 6.4 m and communication with 4% packet loss over 7 m.

Two early versions of AquaOptical are presented in [14]. The first is a miniaturized version capable of error-free communication in ocean water at data rates of 4 Mb/s over a distance of 2.2 m (470 nm) and 2.4 m (532 nm). It uses a Luxeon V LED at either 470 nm (480 mW) or 532 nm (700 mW) and a PDB-C156 PD. The second version of AquaOptical presented is a transmitter/receiver pair using an array of six such LEDs to increase transmit power and an avalanche PD to increase receiver sensitivity. The APD is an Advanced Photonix 5 mm^2 area Silicon APD coupled with an LNA (part number SD197-70-74-661). We evaluate the modem in the Singapore Harbor at a data rate of 600 kb/s with error-free communication at a distance of 7 m and BER of 0.05 at 8 m. The water quality was estimated

by divers to yield about 5 e-folding lengths at 8 m. In [7], we demonstrate the use of AuqaOptical for AUV teleoperation.

In [22], we present a bidirectional version, called AquaOptical II, which uses 18 Luxeon Rebel LEDs and the same APD as the previous version. The LEDs transmit at a wavelength of 470 nm with up to 1.126 W of radiant flux each, resulting in a total transmit power of 20 W. An FPGA is used for PHY processing, and an ARM7TDMI processor handles the MAC and provides an external 10-Mb/s Ethernet interface. We demonstrate communication at a data rate of 4 Mb/s at a distance of up to 50 m in a pool. In a laboratory setting transmitting through air, 32 Mb/s are achieved using non-return-to-zero (NRZ) amplitude modulation with 2 b/symbol. In [1], we use AquaOptical II in a data muling application where the robot estimates its position relative to a sensor node based on measured optical signal strength and simultaneously downloads payload data.

VII. Conclusion and Future Work

We have presented a generic model of signal strength in underwater optical communications. This model allows estimation of receiver signal strength dependent on transmission angles, transmission distance, and a receiving angle. It takes into account all relevant components of an underwater optical modem as well as propagation through the water. Using the model, we predicted signal strength for AquaOptical II. We then collected signal strength measurements experimentally and compared them to the values predicted. For AquaOptical II, the model prediction error was no more than 1.8 dB for transmitter and receiver angles between $-15°$ and $15°$ and distances between 10 and 50 m.

For future work, we would like to further analyze the source of the prediction errors observed when the receiver was held at an angle greater than $\pm 15°$. Additionally, we would like to apply this model to other optical modems.

Acknowledgment

The authors would like to thank A. Anwar, M. Glombicki, M. Volkov, and A. Xu, whose help with the logistics of conducting their pool experiments have been invaluable, and to N. Norris for proofreading.

References

[1] M. W. Doniec, I. Topor, M. Chitre, and D. Rus, "Autonomous, localization-free underwater data muling using acoustic and optical communication," in *Experimental Robotics*, ser. Tracts in Advanced Robotics. New York, NY, USA: Springer-Verlag, 2013, vol. 88, pp. 841–857.

[2] Y. Tsuchida, N. Hama, and M. Takahata, "An optical telemetry system for underwater recording of electromyogram and neuronal activity from non-tethered crayfish," *J. Neurosci. Methods*, vol. 137, no. 1, pp. 103–109, 2004.

[3] F. Schill, U. R. Zimmer, and J. Trumpf, "Visible spectrum optical communication and distance sensing for underwater applications," in *Proc. Australasian Conf. Robot. Autom.*, 2004.

[4] I. Vasilescu, P. Varshavskaya, K. Kotay, and D. Rus, "Autonomous modular optical underwater robot (AMOUR) design, prototype and feasibility study, robotics and automation," in *Proc. IEEE Int. Conf. Robot. Autom.*, 2005, pp. 1603–1609.

[5] M. Dunbabin, P. Corke, I. Vasilescu, and D. Rus, "Data muling over underwater wireless sensor networks using an autonomous underwater vehicle, robotics and automation," in *Proc. IEEE Int. Conf. Robot. Autom.*, 2006, pp. 2091–2098.

[6] N. Farr, J. Ware, C. Pontbriand, T. Hammar, and M. Tivey, "Optical communication system expands CORK seafloor observatory's bandwidth," in *Proc. OCEANS Conf.*, 2010, DOI: 10.1109/OCEANS.2010.5663951.

[7] M. Doniec, C. Detweiler, I. Vasilescu, and D. Rus, "Using optical communication for remote underwater robot operation," in *Proc. IEEE/RSJ Int. Conf. Intell. Robots Syst.*, 2010, pp. 4017–4022, DOI: 10.1109/IROS.2010.5650224.

[8] M. Chancey, "Short range underwater optical communication links," M.S. thesis, Dept. Electr. Eng., North Carolina State Univ., Raleigh, NC, USA, 2005.

[9] F. Hanson and S. Radic, "High bandwidth underwater optical communication," *Appl. Opt.*, vol. 47, no. 2, pp. 277–283, 2008.

[10] S. Jaruwatanadilok, "Underwater wireless optical communication channel modeling and performance evaluation using vector radiative transfer theory," *IEEE J. Sel. Areas Commun.*, vol. 26, no. 9, pp. 1620–1627, Dec. 2008.

[11] J. Giles and I. Bankman, "Underwater optical communications systems. Part 2: Basic design considerations," in *Proc. IEEE Military Commun. Conf.*, 2005, vol. 3, pp. 1700–1705, DOI: 10.1109/MILCOM.2005.1605919.

[12] C. Gabriel, M. Khalighi, S. Bourennane, P. Leon, and V. Rigaud, "Channel modeling for underwater optical communication," in *Proc. IEEE GLOBECOM Workshop*, 2011, pp. 833–837, DOI: 10.1109/GLOCOMW.2011.6162571.

[13] D. Kedar and S. Arnon, "Non-line-of-sight optical wireless sensor network operating in multiscattering channel," *Appl. Opt.*, vol. 45, no. 33, pp. 8454–8461, 2006, DOI: 10.1364/AO.45.008454.

[14] M. Doniec, C. Detweiler, I. Vasilescu, M. Chitre, M. Hoffman-Kuhnt, and D. Rus, "AquaOptical: A lightweight device for high-rate long-range underwater point-to-point communication," *Mar. Technol. Soc. J.*, vol. 44, no. 4, pp. 55–65, 2010.

[15] M. Bass, C. DeCusatis, J. Enoch, V. Lakshminarayanan, G. Li, C. Macdonald, V. Mahajan, and E. Van Stryland, *Handbook of Optics, Third Edition Volume II: Design, Fabrication and Testing, Sources and Detectors, Radiometry and Photometry*, 3rd ed. New York, NY, USA: McGraw-Hill, 2010, ch. 24, p. 14, eq. (21) and (22).

[16] J. T. O. Kirk, "Estimation of the absorption and the scattering coefficients of natural waters by use of underwater irradiance measurements," *Appl. Opt.* vol. 33, no. 15, pp. 3276–3278, 1994, DOI: 10.1364/AO.33.003276.

[17] P. S. Saini and S. Prince, "Underwater optical wireless channel modeling using Monte-Carlo method," in *Proc. AIP Conf.*, 2011, vol. 1391, no. 1, pp. 380–382.

[18] L. Mullen, "Optical propagation in the underwater environment," *Atmos. Propag.*, vol. VI, pp. 732409–732409-9, 2009, DOI: 10.1117/12.820205.

[19] P. Lacovara, "High-bandwidth underwater communications," *Mar. Technol. Soc. J.*, vol. 42, no. 1, pp. 93–102, 2008, DOI: 10.4031/002533208786861326.

[20] M. Lanzagorta, "Underwater communications," *Synthesis Lectures Commun.*, vol. 5, no. 2, pp. 1–129, 2012.

[21] L. Sharpe, A. Stockman, W. Jagla, and H. Jgle, "A luminous efficiency function, $v*(\lambda)$, for daylight adaptation," *J. Vis.*, vol. 5, no. 11, Dec. 2005, DOI: 10.1167/5.11.3.

[22] M. Doniec and D. Rus, "Bidirectional optical communication with AquaOptical II," in *Proc. IEEE Int. Conf. Commun. Syst.*, 2010, pp. 390–394, DOI: 10.1109/ICCS.2010.5686513.

[23] N. Farr, A. Chave, L. Freitag, J. Preisig, S. White, D. Yoerger, and P. Titterton, "Optical modem technology for seafloor observatories," in *Proc. MTS/IEEE OCEANS Conf.*, 2005, vol. 1, pp. 928–934, DOI: 10.1109/OCEANS.2005.1639874.

[24] N. Farr, A. Chave, L. Freitag, J. Preisig, S. White, D. Yoerger, and F. Sonnichsen, "Optical modem technology for seafloor observatories," in *Proc. OCEANS Conf.*, 2006, DOI: 10.1109/OCEANS.2006.306806.

[25] C. Pontbriand, N. Farr, J. Ware, J. Preisig, and H. Popenoe, "Diffuse high-bandwidth optical communications," in *Proc. OCEANS Conf.*, 2008, DOI: 10.1109/OCEANS.2008.5151977.

[26] N. Farr, A. Bowen, J. Ware, C. Pontbriand, and M. Tivey, "An integrated, underwater optical/acoustic communications system," in *Proc. IEEE OCEANS Conf.*, 2010, DOI: 10.1109/OCEANSSYD.2010.5603510.

[27] R. Camilli, A. Bowen, and N. Farr, "Bright blue: Advanced technologies for marine environmental monitoring and offshore energy," in *Proc. IEEE OCEANS Conf.*, 2010, DOI: 10.1109/OCEANSSYD.2010.5603892.

[28] R. Agishev, B. Gross, F. Moshary, A. Gilerson, and S. Ahmed, "Simple approach to predict APD/PMT LIDAR detector performance under sky background using dimensionless parametrization," *Opt. Lasers Eng.*, vol. 44, no. 8, pp. 779–796, 2006.
[29] W. Cox, "A 1 mbps underwater communication system using a 405 nm laser diode and photomultiplier tube," M.S. thesis, Dept. Electr. Eng., North Carolina State Univ., Raleigh, NC, USA, 2008.
[30] W. Cox, J. Simpson, C. Domizioli, J. Muth, and B. Hughes, "An underwater optical communication system implementing Reed-Solomon channel coding," in *Proc. OCEANS Conf.*, 2008, DOI: 10.1109/OCEANS.2008.5151992.
[31] J. Simpson, W. Cox, J. Krier, B. Cochenour, B. Hughes, and J. Muth, "5 mbps optical wireless communication with error correction coding for underwater sensor nodes," in *Proc. OCEANS Conf.*, 2010, DOI: 10.1109/OCEANS.2010.5664429.
[32] J. Simpson, B. Hughes, and J. Muth, "A spatial diversity system to measure optical fading in an underwater communications channel," in *Proc. MTS/IEEE OCEANS Conf.*, 2009, pp. 1–6.
[33] W. Cox, K. Gray, J. Simpson, B. Cochenour, B. Hughes, and J. Muth, "A MEMS blue/green retroreflecting modulator for underwater optical communications," in *Proc. OCEANS Conf.*, 2010, DOI: 10.1109/OCEANS.2010.5664432.
[34] W. Cox, J. Simpson, and J. Muth, "Underwater optical communication using software defined radio over led and laser based links," in *Proc. Military Commun. Conf.*, 2011, pp. 2057–2062, DOI: 10.1109/MILCOM.2011.6127621.
[35] B. Cochenour, L. Mullen, A. Laux, and T. Curran, "Effects of multiple scattering on the implementation of an underwater wireless optical communications link," in *Proc. OCEANS Conf.*, 2006, DOI: 10.1109/OCEANS.2006.306863.
[36] B. Cochenour, L. Mullen, and A. Laux, "Phase coherent digital communications for wireless optical links in turbid underwater environments," in *Proc. OCEANS Conf.*, 2007, DOI: 10.1109/OCEANS.2007.4449173.
[37] B. Cochenour and L. Mullen, "Channel response measurements for diffuse non-line-of-sight (NLOS) optical communication links underwater," in *Proc. OCEANS Conf.*, 2011, pp. 1–5.
[38] D. Anguita, D. Brizzolara, and G. Parodi, "Building an underwater wireless sensor network based on optical communication: Research challenges and current results," in *Proc. 3rd Int. Conf. Sensor Technol. Appl.*, 2009, pp. 476–479, DOI: 10.1109/SENSORCOMM.2009.79.
[39] D. Anguita, D. Brizzolara, and G. Parodi, "Optical wireless communication for underwater wireless sensor networks: Hardware modules and circuits design and implementation," in *Proc. OCEANS Conf.*, 2010, DOI: 10.1109/OCEANS.2010.5664321.
[40] D. Anguita, D. Brizzolara, G. Parodi, and Q. Hu, "Optical wireless underwater communication for AUV: Preliminary simulation and experimental results," in *Proc. OCEANS Conf.*, 2011, DOI: 10.1109/OceansSpain.2011.6003598.
[41] D. Anguita, D. Brizzolara, and G. Parodi, "VHDL modules and circuits for underwater optical wireless communication systems," *WSEAS Trans. Commun.*, vol. 9, no. 9, pp. 525–552, 2010.
[42] Ambalux, 2012, http://www.ambalux.com.
[43] G. Baiden and Y. Bissiri, "High bandwidth optical networking for underwater untethered telerobotic operation," in *Proc. OCEANS Conf.*, 2007, DOI: 10.1109/OCEANS.2007.4449121.
[44] G. Baiden, Y. Bissiri, and A. Masoti, "Paving the way for a future underwater omni-directional wireless optical communication systems," *Ocean Eng.*, vol. 36, no. 9–10, pp. 633–640, 2009, DOI: 10.1016/j.oceaneng.2009.03.007.
[45] Penguin Automated Systems, Inc., 2012 [Online]. Available: http://www.penguinasi.com
[46] M. Chen, M. Zhou, and T. Li, "The implementation of PPM in underwater laser communication system," in *Proc. Int. Conf. Commun. Circuits Syst.*, 2006, vol. 3, pp. 1901–1903, DOI: 10.1109/ICCCAS.2006.285044.
[47] R. Hagem, D. Thiel, S. O'Keefe, A. Wixted, and T. Fickenscher, "Low-cost short-range wireless optical FSK modem for swimmers feedback," in *Proc. IEEE Sensors Conf.*, 2011, pp. 258–261, DOI: 10.1109/ICSENS.2011.6127036.
[48] F. Lu, S. Lee, J. Mounzer, and C. Schurgers, "Low-cost medium-range optical underwater modem: Short paper," in *Proc. 4th ACM Int. Workshop Underwater Netw.*, 2009, pp. 11:1–11:4, DOI: 10.1145/1654130.1654141.
[49] H. Brundage, "Designing a wireless underwater optical communication system," M.S. thesis, Dept. Mech. Eng., Massachusetts Inst. Technol., Cambridge, MA, USA, 2010.
[50] I. Vasilescu, K. Kotay, D. Rus, M. Dunbabin, and P. Corke, "Data collection, storage, and retrieval with an underwater sensor network," in *Proc. 3rd Int. Conf. Embedded Netw. Sensor Syst.*, 2005, pp. 154–165.

Marek Doniec received the Vordiplom (B.S. degree) in computer science from the Karlsruhe Institute of Technology, Karlsruhe, Germany, in 2004, the M.S. degree in computer science from Yale University, New Haven, CT, USA, in 2007, and the Ph.D. degree in computer science and electrical engineering from the Massachusetts Institute of Technology (MIT), Cambridge, MA, USA, in 2013. For his Ph.D. dissertation, he investigated automated data retrieval from underwater sensor networks using a team of autonomous underwater robots.

He is a Postdoctoral Associate working with N. Roy at the Computer Science and Artificial Intelligence Lab (CSAIL), MIT. His research interests include robotics, instrumentation, sensor networks, underwater wireless optical communication, and multirobot systems. He has been an active member of research labs in the United States, Germany, France, and Singapore. Additionally, he has experience in industry, having worked at Rethink Robotics, developing controls for a humanoid arm. His work focused on finding nodes whose location is not known precisely and on wirelessly downloading all available payload data before a robot heads on to the next node. For this purpose, he developed and implemented a state-of-the-art wireless underwater communication system. Previously, he contributed to autonomous data gathering in herds of cattle; learning hand–eye coordination for humanoid robots; system-on-a-chip simulation; and brain–computer interfaces.

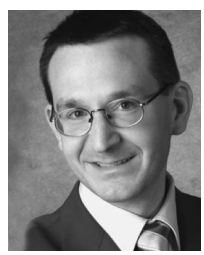

Michael Angermann (S'00–M'04) received the Diplom-Ingenieur degree from the Technische Universität München (TUM), Munich, Germany, in 1998 and the Doktor-Ingenieur degree from the University of Ulm, Ulm, Germany, in 2004.

He is a Research Scientist at the Institute of Communications and Navigation, German Aerospace Center (DLR), Wessling, Germany. He teaches at TUM and the University of the Federal Armed Forces, Munich, Germany. He spent a research semester at the Computer Science and Artificial Intelligence Lab (CSAIL), Massachusetts Institute of Technology (MIT), Cambridge, MA, USA, in 2008. His research interests are in Bayesian methods with applications in communication, localization, mapping, and general context estimation of humans and multiagent robotic systems.

Daniela Rus (S'92–M'92–SM'08–F'10) received the Ph.D. degree in computer science from Cornell University, Ithaca, NY, USA, in 1992.

She is a Professor of Electrical Engineering and Computer Science and an Associate Director of the Computer Science and Artificial Intelligence Lab (CSAIL), Massachusetts Institute of Technology (MIT), Cambridge, MA, USA, and codirects the MIT Center for Robotics at CSAIL. Her research focuses on the science of autonomy for groups of robots and includes applications to transportation, security, environmental modeling and monitoring, underwater exploration, and agriculture. She has spearheaded research in programmable matter by developing the several self-configuring robots.

Prof. Rus is the recipient of the National Science Foundation (NSF) Career Award and an Alfred P. Sloan Foundation Fellow. She is a Class of 2002 MacArthur Fellow and a Fellow of the Association for the Advancement of Artificial Intelligence (AAAI).